Supplementary Information - Appendix

Table S1. Functional parameters of labeled and unlabeled MV constructs.

Functional Parameter	Construct				
	MV	MV.QSY	MV-F.QSY	MV-F.IAANS	MV-F.QSY$_N$
[a]k_{cat} (sec^{-1})	9.7±0.2	9.2±0.1	6.2±0.1	8.0±0.4	7.9±0.3
[a]K_{ATPase} (μM)	2.3±0.2	2.4±0.1	1.8±0.1	2.8±0.6	1.6±0.2
[b]Motility (nm/sec)	409±6	405±6	392±7	385±4	430±5

[a]Determined by fitting the data in Figure S1 to the Michaelis-Menten equation. Errors are reported as standard error of the fit.

[b]Determined with the in vitro motility assay (mean±standard error, n=30-40 actin filaments)

Table S2. Time-resolved FRET* parameters for MV-F.QSY.

TR-FRET Parameter name	Value	STD. Error.	Lower Conf. Bounds	Upper Conf. Bounds
Donor Lifetime Distribution				
Amplitude Tau 1	0.380	0.055	0.372	0.381
Tau 1	3.039	0.146	2.963	3.104
Amplitude Tau 2	0.620	0.056	0.611	0.625
Tau 2	5.061	0.101	4.989	5.123
Post-Power Stroke Distance (nm)				
Distance	3.740	0.012	3.434	3.852
FWHM	2.230	0.055	1.361	3.475
Sigma	0.947	0.023	0.578	1.476
Pre-Power Stroke Distance (nm)				
Distance	6.600	0.035	6.405	6.896
FWHM	0.385	0.800	n/a	2.635
Sigma	0.164	0.340	n/a	1.119
Mole Fraction of FRET				
Mole Fraction Donor in Total	0.337	0.002	0.273	0.401
Mole Fraction FRET in Total	0.663	0.002	0.537	0.789
Mole Fraction Post-Power Stroke In FRET Only				
Apo	0.736	0.003	0.644	0.848
ADP	0.634	0.005	0.433	0.864
ATP	0.425	0.003	0.204	0.582
Actin ADP	0.996	0.005	0.732	n/a
Actin	1.000	0.003	0.783	n/a

***Information about the key parameters (e.g. k^2 and R_0) used to calculate the reported FRET distances are further described on pages 16-21 of the supplemental information.**

Table S3. Anisotropy values for MV-F

Anisotropy Parameter	Apo	ATP	ADP	AM.ADP	AM
Initial Anisotropy	0.35 ± 0.01	0.35 ± 0.01	0.35 ± 0.01	0.35 ± 0.01	0.35 ± 0.01
Correlation Time Nanoseconds	1.98 ± 0.18	2.21± 0.29	2.17 ± 0.26	2.00 ± 0.25	2.62 ± 0.25
Final Anisotropy Fraction Initial	0.75 ± 0.01	0.74 ± 0.02	0.71 ± 0.02	0.76 ± 0.01	0.67 ± 0.02
Final Anisotropy	0.26 ± 0.01	0.26 ± 0.01	0.25 ± 0.01	0.26 ± 0.01	0.23 ± 0.01
Apparent Anisotropy	0.17	0.18	0.17	0.17	0.18

Table S4. Anisotropy values for MV.Rho-CaM (CaM labeled with Tetramethylrhodamine at T110C)

Anisotropy Parameter	Apo	ATP	ADP	AM.ADP	AM
Initial Anisotropy	0.28 ± 0.01	0.28 ± 0.01	0.28 ± 0.01	0.28 ± 0.01	0.28 ± 0.01
Correlation Time Nanoseconds	3.2 ± 0.16	3.38 ± 0.24	3.54 ± 0.32	3.34 ± 0.36	3.25 ± 0.27
Final Anisotropy Fraction Initial	0.34 ± 0.02	0.3 ± 0.03	0.28 ± 0.03	0.26 ± 0.04	0.32 ± 0.03
Final Anisotropy	0.10 ± 0.01	0.08 ± 0.01	0.08 ± 0.01	0.07 ± 0.01	0.09 ± 0.01
Apparent Anisotropy	0.16	0.16	0.17	0.16	0.16

Table S5. Summary of rate and equilibrium constants measured.

Rate or Equilibrium Constant	MV-F.QSY	MV	MV-F.IAANS
[a]Recovery Stroke (k_{+3A})	330±7 sec^{-1}		312 ± 12 sec^{-1}
[b]ATP Binding (k_{+3A})		332±28 sec^{-1}	
[c]Actin Binding in M.ADP.Pi (K_9)	k_{on} = 100 $\mu M^{-1}sec^{-1}$ k_{off} = 2000 sec^{-1}		
[d]Fast Power Stroke (k'_{+4A})	352±33 sec^{-1}		493±119 sec^{-1}
[e]Phosphate Release (k'_{+4B})	201±11 sec^{-1}		
[f]Slow Power Stroke (k'_{+5A})	18±9 sec^{-1}		20±13 sec^{-1}
[g]ADP isomerization (k'_{+5B})	5.3 ± 0.3 sec^{-1}		
[g]ADP-release (k'_{+5C})	32 ± 0.1 sec^{-1}		
[h]ADP-Binding (k'_{-5C})	7.2±0.6 $\mu M^{-1}sec^{-1}$		7.8±1.2 $\mu M^{-1}sec^{-1}$

[a]Maximum rate of ATP binding measured by FRET

[b]Maximum rate observed from the intrinsic tryptophan fluorescence signal

[c]Estimated (Kintek explorer simulation) from the actin dependence of the FRET signal observed upon binding to actin in the M.ADP.Pi state (sequential mix)

[d]Maximum rate of the fast phase from the FRET signal observed upon binding to actin in the M.ADP.Pi state (sequential mix)

[e]Maximum rate of the fluorescence change in the PBP signal observed upon binding to actin in the M.ADP.Pi state (sequential mix)

[f]Average rate of the slow phase from the FRET signal observed upon binding to actin in the M.ADP.Pi state (sequential mix)

[g]Determined from the FRET signal observed upon mixing AM.ADP with saturating ATP

[h]Determined from the FRET signal observed upon ADP binding to AM

Figure S1. **Functional characterization of MV constructs.** Functional parameters were measured for the labeled and unlabeled MV constructs. The maximal rate of ATPase (k_{cat}) and actin concentration at which ATPase activity is one-half maximal (K_{ATPase}) were measured for the unlabeled and the labeled constructs by the NADH-linked ATPase assay at 25°C. The *in vitro* motility rates for these constructs were measured at 26°C. See Table S1 for summary of ATPase and motility parameters.

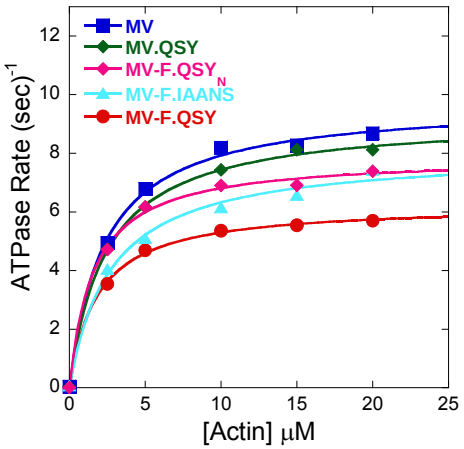

Fig. S2. **Single turnover without actin**. We mixed (0.25 μM) MV-F.QSY with sub-stoichiometric ATP (0.2 μM) and monitored the FRET for a 200 second period. The large FlAsH fluorescence increase was followed by a fluorescence decrease. The last 50 sec. of the fluorescence decrease was fit to a single exponential and found to be similar to the ATPase rate in the absence of actin (0.020 ± 0.001 sec^{-1}).

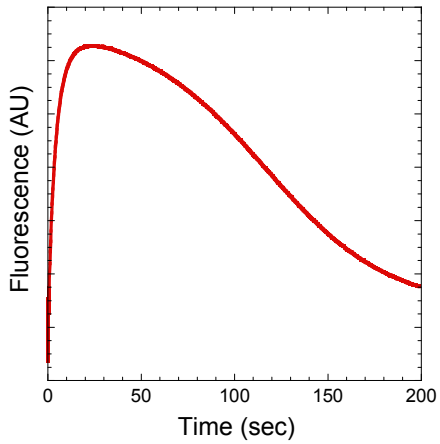

Figure S3. **Rate of Recovery and powerstroke in the MV-F.QSY$_N$ construct.** The rate constant of lever arm swing during the recovery (A&C) and the powerstroke (B&D) was measured with the MV-F.QSY$_N$ construct. The fluorescence transients for both experiments are fit to a double exponential function (A and B inset). The relative amplitudes of the slow phase and fast phases of the recovery stroke (C) and power stroke (D) are shown. The observed rate constant of the fast phase of the recovery stroke is plotted as a function of the ATP concentration and fit to a hyperbola, which allowed determination of the recovery stroke rate constant (311±11 sec^{-1}) (A). In the power stroke measurements the observed rate of the fast phase increased as a function of actin concentration while the observed rate of the slow phase remained unchanged (B). The rate constant of the fast power stroke was 290±64 sec^{-1} while the average rate constant of the slow power stroke was 12±3 sec^{-1}. Insets show the increase and decrease in FlAsH fluorescence during the recovery (A) and power strokes (B), respectively. The recovery stroke trace is in the presence of 50 μM ATP and the power stroke trace is in the presence of 20 μM actin.

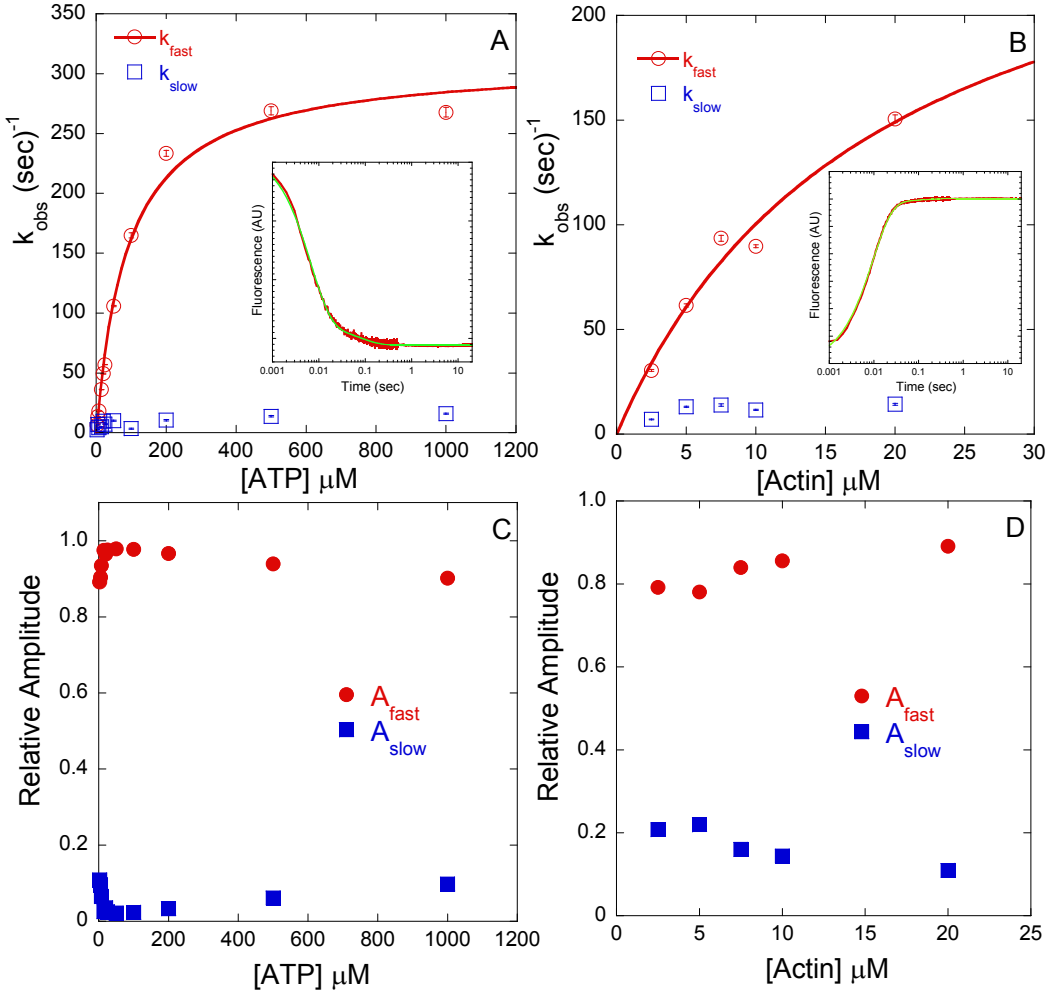

Figure S4. Kinetic simulations of the power stroke and Pi release. Fluorescence transients of the fast phase of the lever arm swing during the power stroke were fit to two models. In model 1 the fast phase of the lever arm swing precedes Pi release (see Scheme 3 and Table S5 for rate constants used in the simulation of model 1) while in model 2 (inset) the lever arm swing and Pi release occur concurrently (same as model 1, except k'_{+4} is a single step that occurs at 201 sec^{-1}).

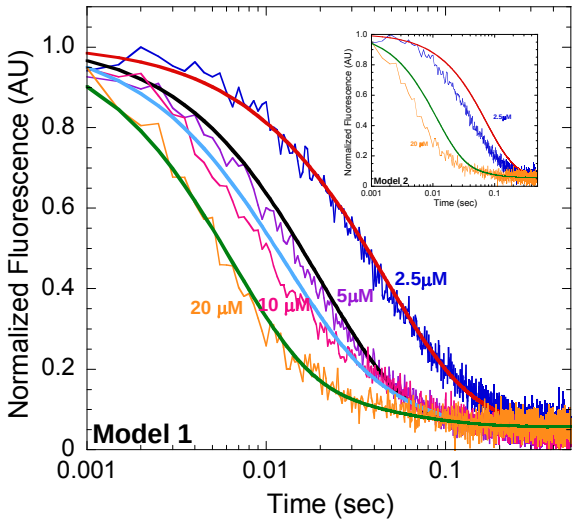

Figure S5. **Kinetics of MV-F binding to pyrene actin in the ADP.Pi state.** The observed rate of pyrene fluorescence quenching upon mixing MV-F.ADP.Pi with different concentrations of pyrene actin was measured. A) The observed rate constant was hyperbolically dependent on pyrene actin concentration and reached a maximal rate of 32±4 sec^{-1}. The fluorescence transients at all concentrations were best fit to a single (green) or double exponential (red, fast phase, slow phase was similar at each actin concentration, ~2 sec^{-1}) function. B) Fluoresence transients observed in the presence or absence of ADP (green trace, 3 μM pyrene actin, 10 μM ATP, 0.1 μM MV-F; red trace, 2.5 μM pyrene actin, 10 μM ATP, 0.25 μM MV-F, and 0.5 mM ADP).

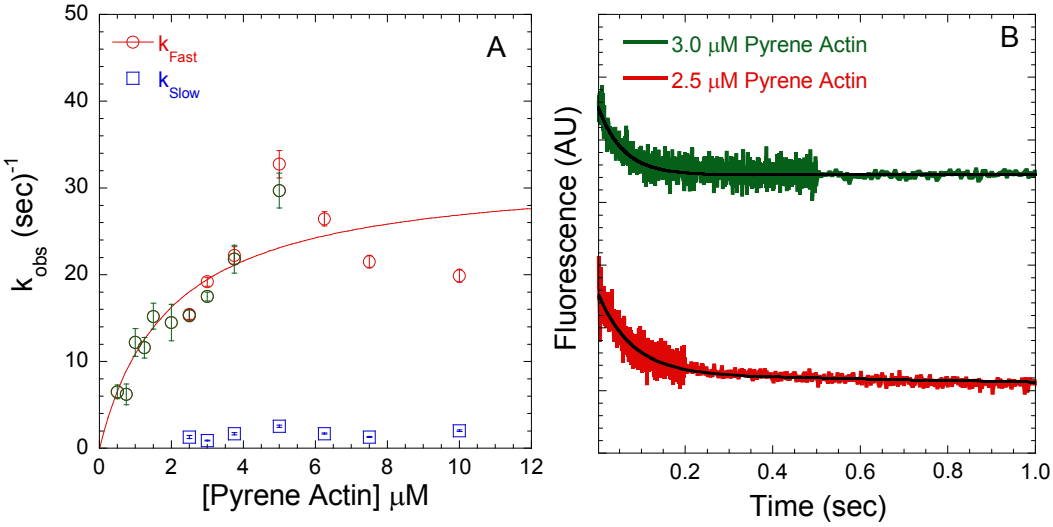

Figure S6: Kinetics of the lever arm swing during the ADP binding and release steps. The lever arm swing during ADP binding was measured by mixing 0.25μM MV-F.QSY (A) or 0.25μM MV-F.IAANS (B) in the presence of actin with different concentrations of ADP. A biphasic fluorescence increase (5 μM ADP, A, upper inset) or a fluorescence decrease (10 μM ADP, B, inset) was observed with the two constructs, respectively. The observed rate of the fast phase increased linearly with the ADP concentration and the second-order binding constants for the FlAsH-QSY and FlAsH-IAANS constructs were 7.2 $\mu M^{-1}sec^{-1}$ and 7.8 $\mu M^{-1}sec^{-1}$ respectively. The ADP-associated isomerization of the NBP was measured by mixing a pre-equilibrated mixture of acto-MV-F.QSY(ADP) with 2mM ATP. A biphasic increase in fluorescence with fast and slow phases of 32±0.1 sec^{-1} and of 5.3±0.3 sec^{-1}, respectively, was observed (A, lower inset). (C) The relative amplitudes of the FRET signal observed with mixing MV-F.IAANS (0.25 μM) with ADP (blue) or ATP (red) (7.5 μM) (the amplitude was about 8- to 10-fold lower in the presence ADP).

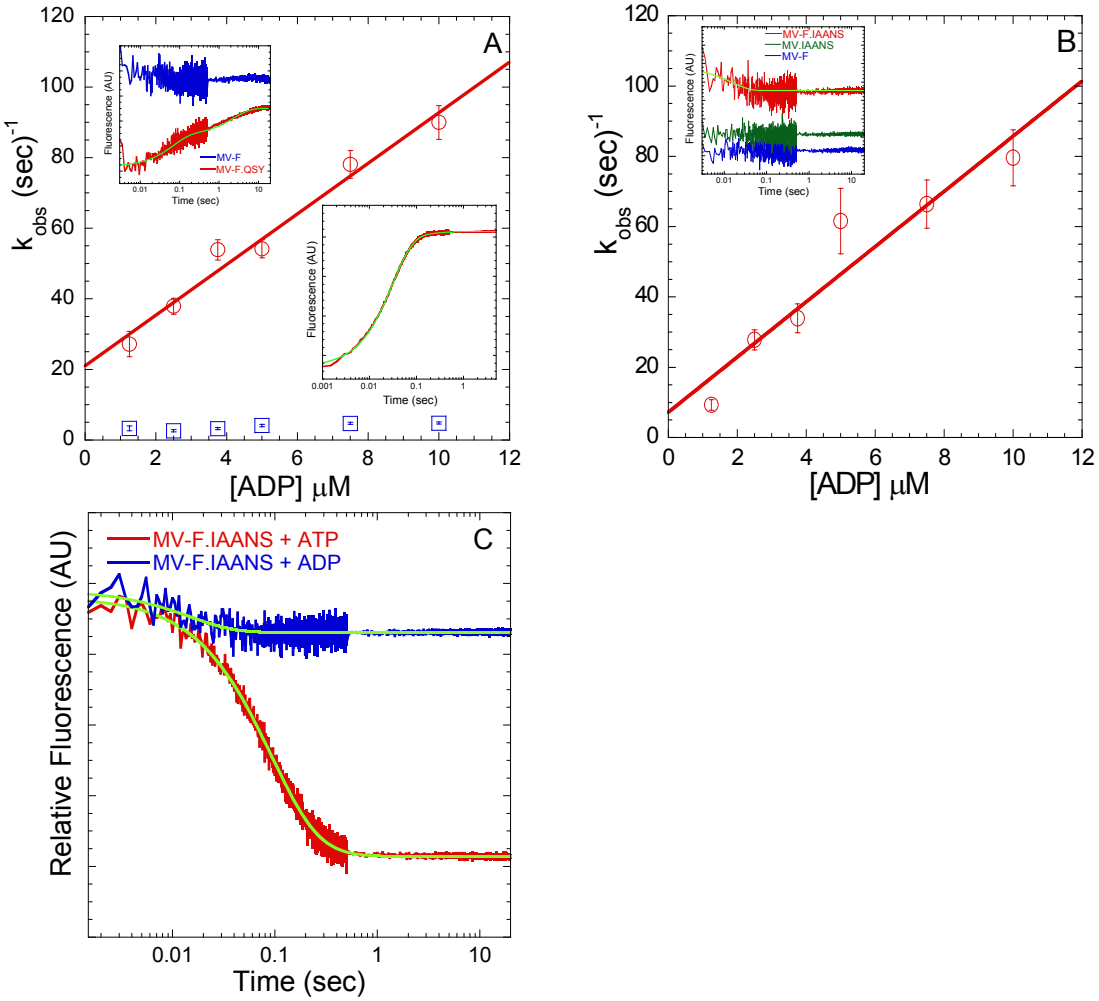

Figure S7. Time-resolved FRET of FlAsH/QSY-9 labeled Myosin V (MV-F.QSY). A) Representative time-resolved fluorescence waveforms of donor only labeled MV under indicated biochemical conditions showing that the waveforms do not change with the varied ligand binding state of MV. B) Representative time-resolved fluorescence waveforms of donor + acceptor labeled MV under indicated biochemical conditions. Concentrations were 0.1 μM MV-F or MV-F.QSY, 2 μM actin, 1 mM ADP, and 1 mM ATP, respectively (25 °C).

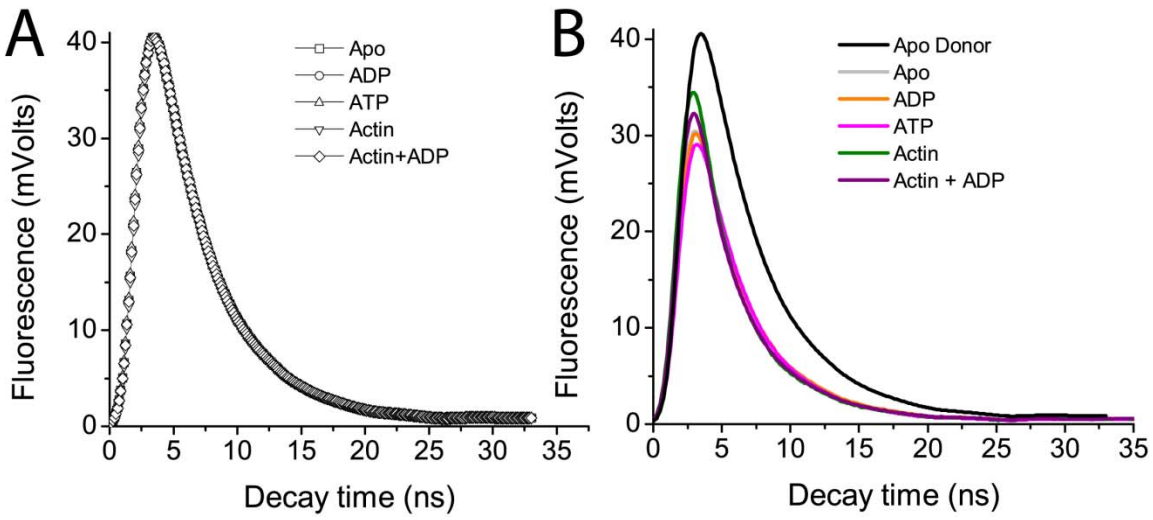

Figure S8. Best-fit model determination of TR-FRET data. Non-linear optimization was used to simultaneously fit donor only and donor + acceptor samples (representative waveforms shown in Fig. S7) with a range of structure based TR-FRET models (described in SI Methods). A) Optimized χ2 for global one-state (1gD), independent one state (1iD), global two-state (2gD), global three-state (3gD) and an arbitrarily unconstrained multi-exponential decay (Unlimited). The best-fit model was a global two-state model (2gD) as indicated by the > 3 fold decrease in χ2 between the one-state and two-state models. Increasing complexity beyond the two-state model did not significantly improve the fit as indicated by the fit χ2. B-D) Representative TR-FRET waveforms of donor + acceptor labeled MV in the absence of nucleotide or actin (B, Apo), presence of saturating ATP (C), or ADP (D) shown as symbols. Fits from models in panel A plotted as colored lines, 1gD (black), 1iD (blue), 2gD (green), 3gD (red), Unlimited (magenta). E-G) Data-model for B-D plotted in E-G,respectively, line color indicates model as described for B-D.

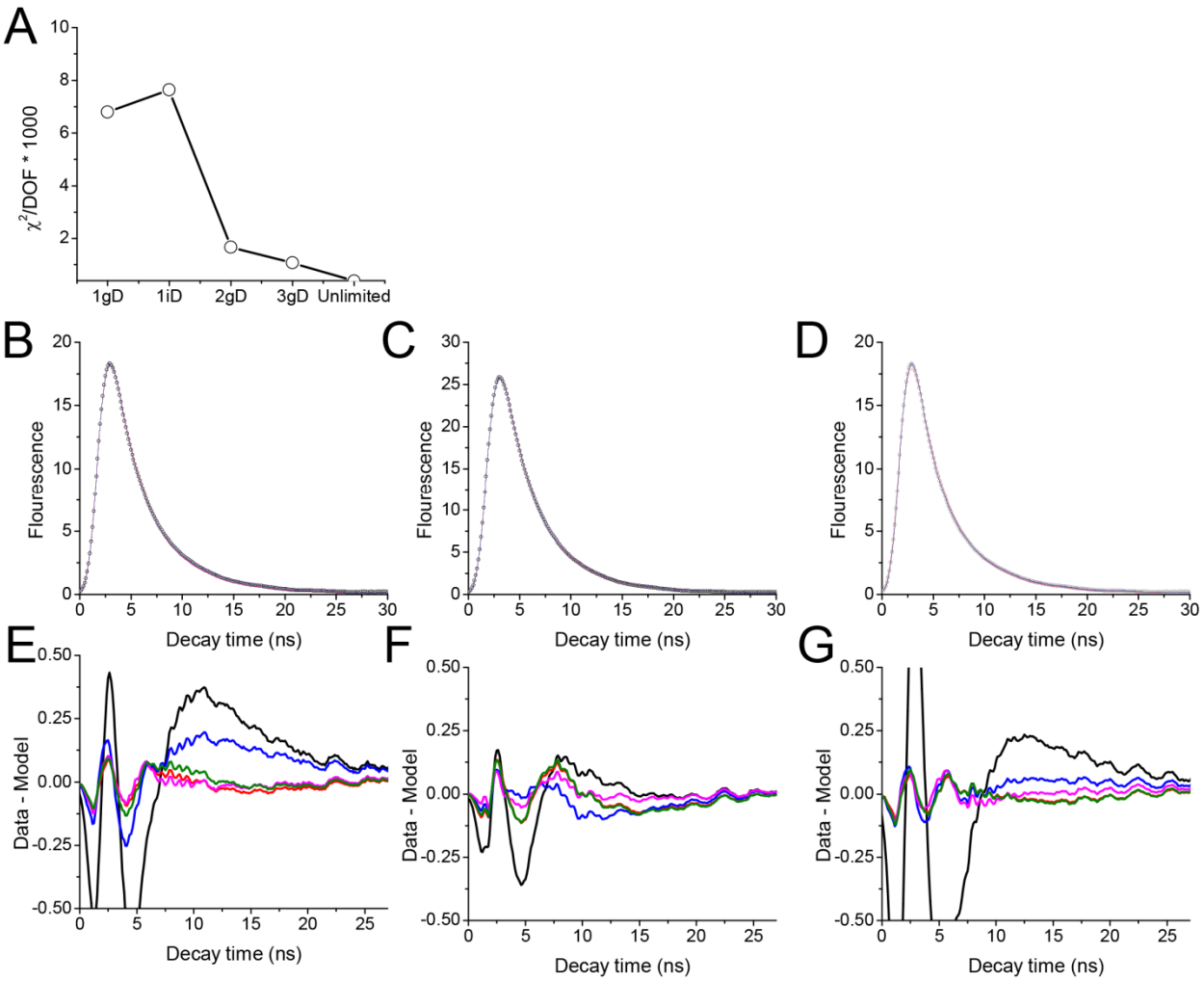

Figure S9. Confidence intervals for distance parameters in the global two-state model (2gD). A) The postpower stroke (R1) correlated short distance structural state Gaussian distribution center or B) standard deviation. C) The prepower stroke (R2) correlated long distance structural state distribution Gaussian distribution center or D) standard deviation. Confidence determined by this analysis is tabulated in Table S2.

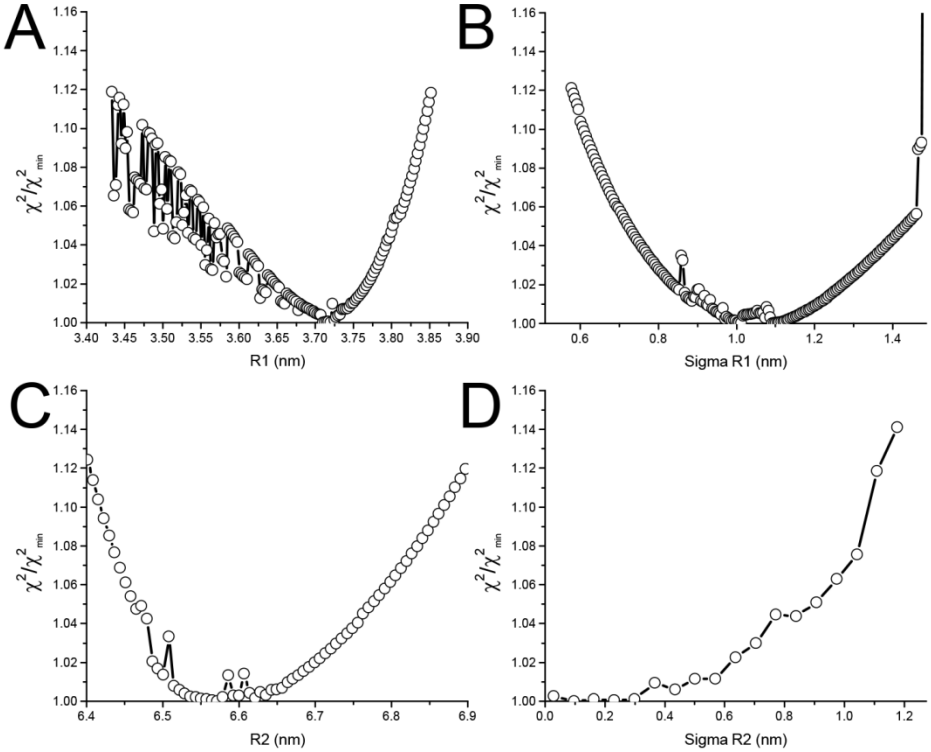

Figure S10. Confidence intervals for the mole fraction of the postpower stroke state under indicated biochemical conditions. Confidence intervals determined by this analysis are tabulated in Table S2. Conditions are as described in Figure S7.

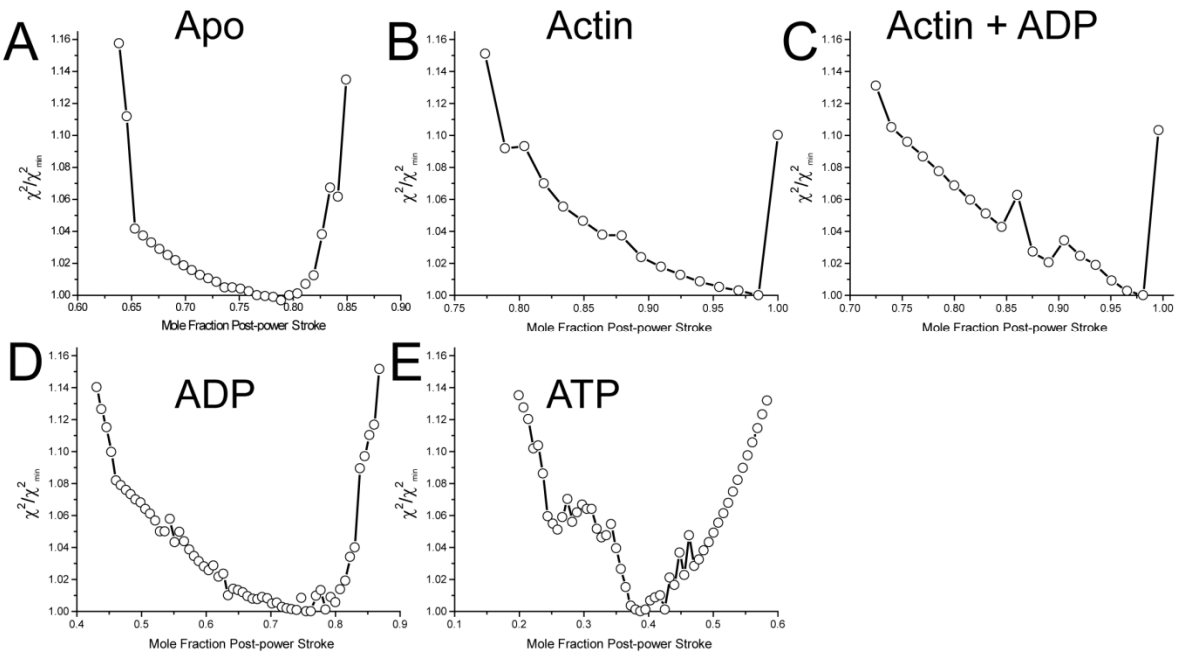

Figure S11. Model of distance change predicted from available crystal structures. The crystal structure of myosin V in the absence of nucleotide (1OE9) (blue) was aligned with the smooth muscle myosin crystal structure in the ADP.BeF_X state (1BR4) (orange) using PyMol alignment. The indicated distance measurements in the post-powerstroke state are from the N-terminus (E5) of MV to the essential light chain residue (T114) that corresponds to the position of T110C of calmodulin. The distance in the pre-power stroke state is from the N-terminus of the aligned myosin V (E5) to essential light chain residue (V113) that corresponds to the position of T110C of calmodulin. The distance was measured from the alpha-carbon of the indicated residues. Location of T5C (corresponding to ELC residue N5) is also shown on the structure for comparison purposes. The distance between the N-terminal FlAsH binding site and T5C in the pre and postpower stroke states is 86.7Å and 44.9Å, respectively.

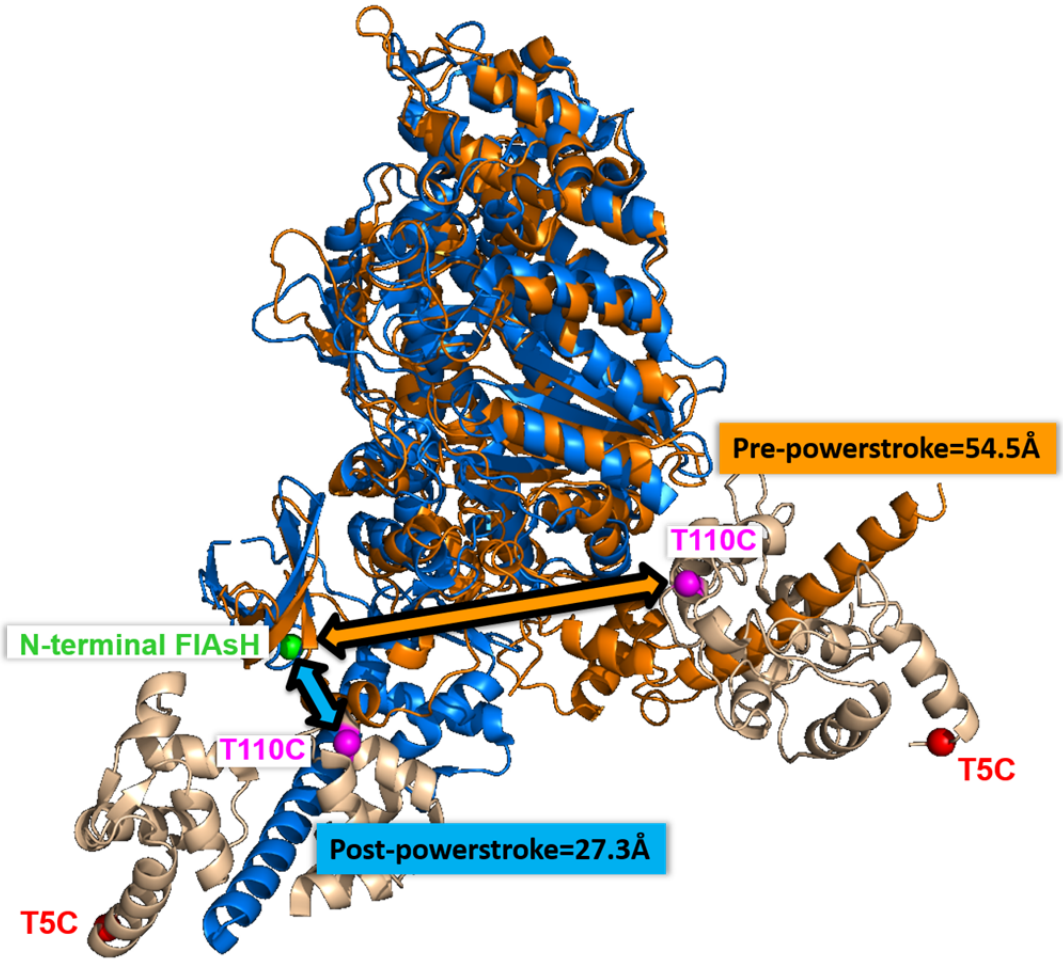

Figure S12. Model of Actomyosin ATPase Cycle. The diagram of the key conformational changes in the actomyosin ATPase cycle is based on the available structural and biochemical studies as well as the FRET studies performed in the current work. ATP binding to AM results in formation of the weak actin binding state (K'_1 and K'_2) which is followed by formation of the hydrolysis competent state and the recovery stroke (K_{3A}) and then hydrolysis (K_{3B}). The steps associated with actin binding and the power stroke are characterized by the M.ADP.Pi complex binding to actin and closure of the actin binding cleft (K_9) which is followed by a rapid conformational change in the lever arm (K'_{4A}) that precedes the release of phosphate (K'_{4A}). After the release of phosphate (K'_{4B}) an additional movement of the lever arm occurs (K'_{5A}) that is faster than the nucleotide binding pocket opening step (K'_{5B}) and precedes the release of ADP (K'_{5C}).

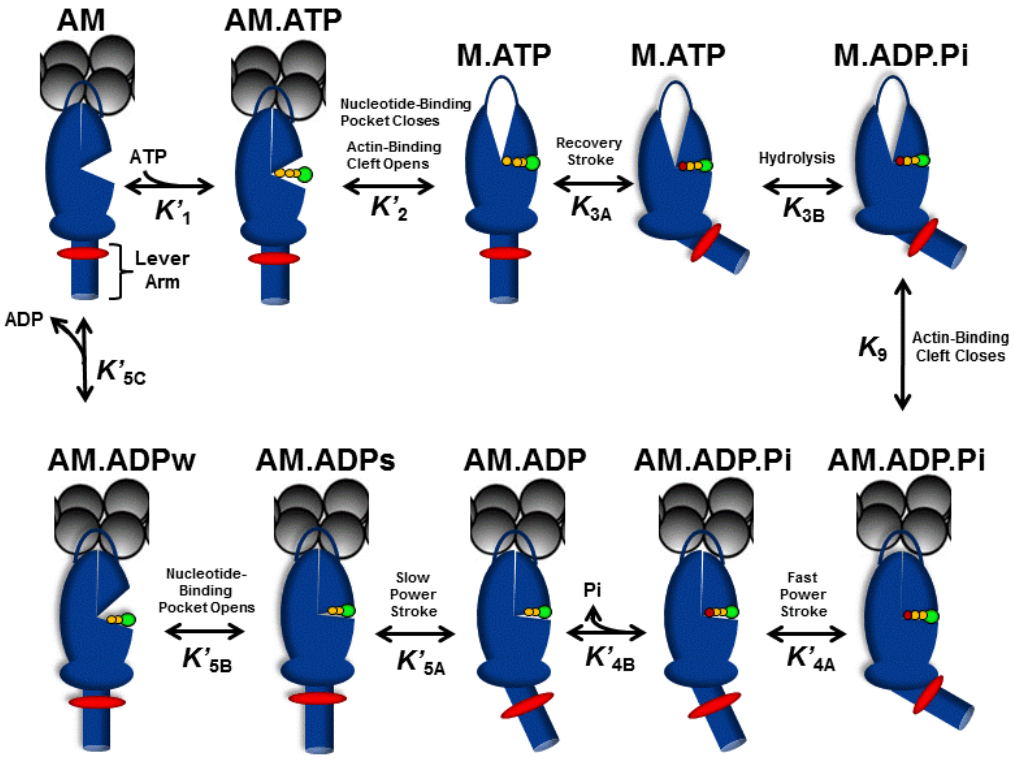

Supplemental Methods

Reagents. Reagents used for all experiments were commercially available and of the highest purity. ATP and ADP stocks were freshly prepared from powder and their concentrations were measured by absorbance at 259nm (ε_{259} = 15,400 $M^{-1}cm^{-1}$). The non-fluorescent acceptor QSY-9 was purchased from Invitrogen (Carlsbad, CA). FlAsH dye was a generous gift from Roger Tsien and Stephen Adams at University of California, San Diego.

ATPase and motility assays. ATPase assays were performed at 25°C in the stopped-flow using the NADH coupled assay and *in vitro* motility assays to measure the actin filament sliding velocity were performed as described (1).

Expression, purification and labeling of calmodulin and myosin V. To generate constructs which measure the lever arm swing, purified MV was stripped of its native Calmodulin (CaM) and QSY or IAANS labeled CaM was exchanged onto the lever arm at the first IQ -motif of MV. We introduced a single cysteine into CaM by substituting the C-terminal threonine 110 with cysteine or substituting the N-terminal threonine 5 with cysteine using site directed mutagenesis. CaM was labeled with the maleimide containing non-fluorescent acceptor QSY 9 by a thiol linkage. CaM was denatured by dialyzing in a urea containing buffer (6M urea, 100mM KCl, 100mM Tris, 1mM EGTA, pH 7.5). Thereafter, the CaM was diluted to 20μM in the urea-buffer followed by labeling with a 10-15 fold excess QSY 9 dye (dissolved in DMF). The reaction proceeded for 15-20 minutes at room temperature and then overnight on ice. The excess dye and urea were removed by exhaustive dialysis in a buffer containing 100mM KCl and 10mM Tris (pH 7.5). The post-dialysed, refolded, QSY- CaM was then passed through a phenyl-sepharose column, to remove any excess dye. The elute was used directly to exchange onto MV, or pooled together and vacuum-dried for later usage. T5C CaM was labeled with the IAANS fluorophore using a protocol described for troponin C (2). A chicken MV construct containing residues 1-792 (single IQ motif) was modified to contain a tetracysteine motif (CCPGCC) on the N-terminal (NT) domain (introduced after the start codon) for FlAsH labeling, and a C-terminal FLAG tag for purification. All MV constructs were expressed in the SF9 cell/baculovirus system (1). QSY or IAANS labeled CaM was exchanged onto the MV constructs during the anti-FLAG affinity column purification step. MV bound to the FLAG resin was initially washed with EGTA containing buffer. This was followed by incubation with wash buffer without EGTA but containing 5mM $CaCl_2$ and 500μM Trifluoroperazine for 30 min. The wash was repeated twice to ensure a total stripping of the native CaMs from the resin-bound MV. The column was returned to EGTA containing wash buffer. A solution of 20-30μM QSY-CaM or IAANS CaM was then added to the resin and allowed to incubate for 1 hr with occasional stirring of the resin. The labeled-CaM was then allowed to flow through, followed by an additional column wash. The MV exchanged with QSY-CaM was then eluted off the column with excess FLAG peptide. FlAsH labeling was performed as described previously (1, 3, 4). Myosin concentrations were measured using the Bio-Rad microplate assay using Bovine Serum Albumin (BSA) as a standard. The extent of labeling with FlAsH or the exchange of labeled CaM was quantified using fluorescent gels and by absorbance measurements. Actin was purified from rabbit skeletal muscle according to the acetone powder method (5).

Stopped-flow measurements. All experiments were performed in KMg50 TCEP buffer (50mM KCl, 1mM EGTA, 1mM $MgCl_2$ 1mM TCEP, 10 mM Imidazole-HCl pH 7.0). A stopped-flow apparatus (Applied Photophysics, Surrey, UK) with a dead-time of 1.2ms was used for all transient kinetic experiments. A monochromator with a 2-nm band pass was used for excitation, and fluorescence emission was measured with cut-off filters provided with the instrument. Tryptophan fluorescence was measured by exciting at 290 nm and emission was measured with a 320 nm long-pass filter. FlAsH fluorescence was excited directly (488 nm) or by energy transfer from IAANS (365 nm) and the emission monitored with a 515 long pass filter. The phosphate-binding protein covalently labeled with *N*-[2-(1-maleimidyl)ethyl]-7-(diethylamino)coumarin-3-carboxamide-(MDCC-PBP) (generously provided by Howard White, Eastern Virginia University School of Medicine) was excited at 380 nm and the emission measured with a 395 long pass filter (6). Data were fit by nonlinear least-squares fitting using the software provided with the instrument. Uncertainties reported are standard error of the fits. All concentrations mentioned in the stopped-flow experiments are final concentrations unless noted otherwise. Kinetic modeling and simulations were performed with Kintek explorer software (Kintek corp.) using the kinetic schemes described in the text.

Time-resolved fluorescence anisotropy data acquisition and analysis. Time-resolved anisotropy measurements of the donor probe used in this study were measured by single photon counting (donor, FlAsH, excited by a 473 nm wavelength pulsed diode laser, pico-quant). The anisotropy of the QSY-9 acceptor, which is not fluorescent, was estimated by measuring the anisotropy of tetramethylrhodamine (TMR) excited at 532 nm with a microchip YAG laser and detected using a custom built time-resolved fluorescence spectrometer, described by Muretta *et. al.* (7). Data acquisition was performed as described (8, 9), measuring the 0^o, 90^o, and 54.7^o, polarized time-resolved fluorescence emission following 0^o polarized excitation.

We analyzed the resulting data following protocols as described (7-9). The measured waveforms were fit by iterative convolution (10) to a system of time-resolved fluorescence equations (Eq, 1-4). We determined the optimum values for parameters in these equations by non-linear optimization in Matlab using the fmincon optimization function, or using software described in our previous reports (7). Parameters for the system of equations were optimized to generate simulated polarized time-resolved fluorescence decays, which were then directly convolved with the measured instrument response function (7, 10) detected by acquiring the excitation pulsed scattered by water. The convolution was performed using a direct integration algorithm validated in our previous work (7). This integration can also be performed using the "filter" function available in Matlab.

We varied the number of fluorescence lifetimes, τ_i, (Eq. 1) and rotational correlation times, τ_{Ri}, (Eq. 4) applied to each biochemical condition (apo, ATP, ADP, actin, actin+ADP).

$$F(54.7°, t) = \sum_{i=1}^{3} A_i \, exp(-t/\tau_i) \qquad \text{Eq. 1}$$

$$F\,(0°, t) = F(54.7°,\ t) \cdot [1 + 2r(t)]/3 \qquad \text{Eq. 2}$$

$$F(90°, t) = F(54.7°,\ t) \cdot [1 - 2r(t)]/3 \qquad \text{Eq. 3}$$

$$r(t) = r_\infty + r_i\, exp(-t/\tau_{Ri}) \qquad \text{Eq. 4}$$

The time-resolved fluorescence decays of FlAsH and TMR are best described by bi- exponential decay functions. The anisotropy components in Eq. 1-4, r(t), were best described by a single exponential decay for each fluorescent lifetime. The total anisotropy, r_o, was calculated according to Eq. 5.

$$r_0 = \frac{\int_{-\infty}^{\infty} F(54.7°,\ t) \cdot r(t)dt}{\int_{-\infty}^{\infty} F(54.7°,\ t)dt} \qquad \text{Eq. 5}$$

$$\langle d_P^x \rangle = \sqrt{r_{0P}/r_f} \qquad \text{Eq. 6}$$

$$\langle \kappa^2 \rangle_{min} = \left(\frac{2}{3}\right) \cdot \left(1 - \frac{\langle d_D^x \rangle + \langle d_A^x \rangle}{2}\right) \qquad \text{Eq. 7}$$

$$\langle \kappa^2 \rangle_{max} = \left(\frac{2}{3}\right) \cdot (1 + \langle d_D^x \rangle + \langle d_A^x \rangle + 3\langle d_D^x \rangle \langle d_A^x \rangle) \qquad \text{Eq. 8}$$

$$R_{min,max} = [(3/2) \cdot \langle \kappa 2 \rangle_{min,max}]^{1/6} \cdot R(\kappa 2 = 2/3) \qquad \text{Eq. 9}$$

We calculated probe depolarization factors, d_p^x, (Eq.6), from the total anisotropy Eq 5, assuming the anisotropy of an immobilized assembly of probes, $r_{f,}$ to be 0.4. We assumed that the dark QSY-9 acceptor exhibits similar anisotropy as the fluorescent TMR label attached at the same site. We calculated the maximum uncertainty in the orientation sensitive term κ^2 according to Eq. 7 and Eq. 8 and the maximum uncertainty in the average Ro according to Eq. 9.

Time-Resolved FRET (TR-FRET) acquisition and analysis. We measured time-resolved FRET between the N-terminus of myosin V and T110C of CaM by acquiring time-resolved fluorescence decays of samples labeled with the FlAsH donor (MV-F), or with the FlAsH donor and the QSY-9 acceptor (MV-F.QSY) using a custom time-resolved fluorescence spectrophotometer (7). TR-FRET between donor and acceptor probes were analyzed according to protocols based on (10), outlined in (8) (summarized below).

Measured time-resolved fluorescence waveforms, *I*(t) (Eq 10),

$$I(t) = \int_{-\infty}^{\infty} \mathrm{IRF}(t - t') \cdot F(t')dt' \quad \text{Eq. 10}$$

are dependent on the picosecond to nanosecond timescale, t, following excitation of the excited state, and are modeled as the convolution integral of the measured instrument response function, IRF(t) detected as described above, and the assumed fluorescence decay model, *F*(t) (Eq. 11)

$$F(t) = x_{\mathrm{D}} F_{\mathrm{D}}(t) + (1 - x_{\mathrm{D}})\, F_{\mathrm{DA}}(t) \quad \text{Eq. 11}$$

where, F_D(t) is the donor only decay, and F_{DA}(t) is the time-resolved decay of the donor probe in the presence of acceptor. X_D is the mole fraction of molecules labeled with the donor only and 1-X_D is the mole fraction of molecules labeled with both the donor and the acceptor. The donor decay F_D(t) was modeled as a sum of exponentials (Eq. 12)

$$F_{\mathrm{D}}(t) = \sum_{i=1}^{2} A_{\mathrm{i}}\, exp(-t/\tau_{\mathrm{i}}) \quad \text{Eq. 12}$$

with discrete lifetime species τ_i and pre-exponential mole fractions A_i. For the FlAsH donor, two exponentials were required to fit the observed fluorescence, consistent with our previous work (1). These are summarized in Table S2. We assumed that the energy transfer-affected donor decay function, F_{DA}(t) (Eq. 13)

$$F_{\mathrm{DA}}(t) = \sum_{\mathrm{j}=1}^{2} X_{\mathrm{j}} \cdot T_{\mathrm{j}}(t) \quad \text{Eq. 13}$$

reflects a sum of distinct Gaussian distributions of interprobe distances T_j(t), that report distinct structural states of the myosin V light-chain binding domain, with mole fractions X_j. This assumption is reasonable and gives qualitatively similar results as assuming discrete distances or assuming non-Gaussian distance distributions. The increase in the donor decay rate due to FRET is given by (Eq. 14-16)

$$k_{\mathrm{Ti}} = k_{\mathrm{Di}}(R/R_{0\mathrm{i}})^{-6}, \text{ where} \quad \text{Eq. 14}$$

$$k_{\mathrm{DAi}} = k_{\mathrm{Di}} + k_{\mathrm{Ti}}, \text{and} \quad \text{Eq. 15}$$

$$k_{\mathrm{Di}} = 1/\tau_{\mathrm{i}} \quad \text{Eq. 16}$$

We modeled TR-FRET assuming that each structural state *j* (Eq. 17) corresponds to a Gaussian distribution of interprobe distances, $\rho_j(R)$:

$$T_j(t) = \int_{-\infty}^{\infty} \rho_j(R) \cdot \sum_{i=1}^{2} A_i \, exp\left(\frac{-t}{\tau_i} \cdot \left[1 + \left(\frac{R_{0i}}{R}\right)^6\right]\right) dR \quad \text{Eq. 17}$$

$$\rho_j(R) = \frac{1}{\sigma_j\sqrt{2\pi}} \exp\left(\frac{-\left[R - R_j\right]^2}{2\sigma_j^2}\right) \quad \text{Eq. 18}$$

$$\sigma_j = \mathrm{FWHM}_j/\left(2\sqrt{2\ln 2}\right) \quad \text{Eq. 19}$$

R_0i terms were calculated according to Eq. 20 from the spectral overlap integral, *J*, the orientation-sensitive term κ^2, the refractive index, n, and the donor quantum yield, Q_{Di} (Eq. 21-23). $\langle Q_D \rangle$ was measured as 0.42 ± 0.01, by direct comparison with a known standard and is similar to values reported elsewhere (11, 12). The R_0i was determined to be 55.9 Å.

$$\mathrm{R}_{0i} = 9780[J\,(\lambda)\kappa^2 n^{-4} Q_i]1/6 \quad \text{Eq. 20}$$

$$Q_{Di} = \langle Q_D \rangle \cdot \tau_i / \langle \tau \rangle \quad \text{Eq. 21}$$

$$\langle \tau \rangle = \frac{\sum_{i=1}^{2} A_i \tau_i}{\sum_{i=1}^{2} A_i} \quad \text{Eq. 22}$$

$$\langle Q_D \rangle = Q_S \cdot \left(\frac{F_D(\lambda)}{A_D(\lambda)}\right) \Big/ \left(\frac{F_S(\lambda)}{A_S(\lambda)}\right) \quad \text{Eq. 23}$$

The donor fluorescence (A_i, τ_i) and distance parameters (R_j, σ_j) in our analysis were shared globally between waveforms from labeled myosin V samples acquired over a range of biochemical conditions. The distance-dependent terms R_j (Eq.17) and σ_j (Eq. 18) define structural states post-power stroke (*j* = 1) and pre-power stroke (*j* = 2) of the myosin V lever arm. The mole fraction terms X_1 and X_2 correspond to the post-power stroke and pre-power stroke structural states respectively.

TR-FRET model determination. We determined the best-fit model by comparing the relative χ^2 for increasingly complex models fit as described above. Time-resolved fluorescence waveforms of donor only and donor + acceptor labeled MV (Figure S7) were fit with increasingly complex TR-FRET models (Figure S8). These included a series of global models where the structural state of the MV lever arm exists in defined structural states with the nucleotide and ligand binding state changing the mole fraction of these states. We also tested models where the structural states were unique to each ligand binding state. The global models are referred in Figure S8 as 1gD, 2gD, 3gD while the non-global model tested is referred as 1iD. The number

in this notation indicates the number of structural states prescribed by Gaussian distance distributions. The 1dD and 1iD models fit the data similarly (Figure S8A). Increasing the model complexity to 2gD produced a 3-4 fold decrease in the fit χ^2. Increasing model complexity beyond the 2gD model by adding a third distance or by fitting the data with and arbitrarily complex multi-exponential decay, did not lower the χ^2 significantly, despite the added free parameters in the fit. This analysis suggests that the 2gD model is sufficient to describe the structural state of the MV lever arm detected by TR-FRET over the range of biochemical ligand binding states tested (Apo, ATP, ADP, Actin, Actin-ADP). Representative TR-FRET waveforms for donor + acceptor MV samples under three of these conditions (Apo, ATP, and ADP) where the post-power stroke and pre-power stroke structural states are both clearly present in differing degrees are shown in Figure S8B-D and representative residuals, obtained by fitting the waveforms to the models described for Figure S8A are shown in Figures S8E-G. The 1iD and 1gD models give notably large residuals compared to the 2gD and 3gD models, which exhibit similar magnitudes in the plotted residuals.

We determined the confidence intervals for each parameter in the 2gD model by performing support plane error analysis as described in our previous work (6-7). The confidence intervals, plotted for the distance (Figure S9) and mole-fraction (Figure S10) parameters reveal the maximum uncertainty in each measured parameter. These maximum uncertainties are tabulated in Table S2 as well as the standard error for the fit parameters, which are much lower than the χ^2 support plane.

References

1. Trivedi DV, Muretta JM, Swenson AM, Thomas DD, & Yengo CM (2013) Magnesium impacts myosin V motor activity by altering key conformational changes in the mechanochemical cycle. *Biochemistry* 52(27):4710-4722.
2. Davis JP*, et al.* (2007) Effects of thin and thick filament proteins on calcium binding and exchange with cardiac troponin C. *Biophys J* 92(9):3195-3206.
3. Jacobs DJ, Trivedi D, David C, & Yengo CM (2011) Kinetics and thermodynamics of the rate-limiting conformational change in the actomyosin V mechanochemical cycle. *J Mol Biol* 407(5):716-730.
4. Trivedi DV, David C, Jacobs DJ, & Yengo CM (2012) Switch II Mutants Reveal Coupling between the Nucleotide- and Actin-Binding Regions in Myosin V. *Biophys J* 102(11):2545-2555.
5. Pardee JD & Spudich JA (1982) Purification of muscle actin. *Methods Cell Biol* 24:271-289.
6. Sun M, Rose MB, Ananthanarayanan SK, Jacobs DJ, & Yengo CM (2008) Characterization of the pre-force-generation state in the actomyosin cross-bridge cycle. *Proc Natl Acad Sci U S A* 105(25):8631-8636.
7. Muretta JM*, et al.* (2010) High-performance time-resolved fluorescence by direct waveform recording. *The Review of scientific instruments* 81(10):103101.
8. Muretta JM, Petersen KJ, & Thomas DD (2013) Direct real-time detection of the actin-activated power stroke within the myosin catalytic domain. *Proc Natl Acad Sci U S A* 110(18):7211-7216.
9. Muretta JM*, et al.* (2013) Loop L5 assumes three distinct orientations during the ATPase cycle of the mitotic kinesin Eg5: a transient and time-resolved fluorescence study. *The Journal of biological chemistry* 288(48):34839-34849.
10. Lakowicz JR (2006) *Principles of Fluorescence Spectroscopy* (Springer, New York, NY) 3rd Ed.
11. Rosenfeld SS*, et al.* (2009) The ATPase cycle of the mitotic motor CENP-E. *The Journal of biological chemistry* 284(47):32858-32868.
12. Martin BR, Giepmans BN, Adams SR, & Tsien RY (2005) Mammalian cell-based optimization of the biarsenical-binding tetracysteine motif for improved fluorescence and affinity. *Nature biotechnology* 23(10):1308-1314.